

# Inferring Wind Velocity from Informal Environmental Objects using Optical Flow Informed Recurrent Neural Networks

Yifan Yang, Adolfo Perrusquía, and Weisi Guo

**Abstract**—Due to their flexibility and wide range of applications, UAVs are expected to play an important role in complex urban airspace in the future. However, unpredictable low-level air currents caused by the complexity and variability of local urban design can pose significant risks to the take-off and landing phases. Current high-quality wind profile radars are expensive and only deployed in major airports. The alternative is to conduct large-scale urban modelling of wind using computation fluid dynamics, which relies on a large volume of accurate city and wind profile data. This undermines the future business model of distributed air mobility, e.g., takeoff and land in ad-hoc locations across a city. Therefore, it is crucial to create an approach that is data-efficient and economical. To achieve this, we leverage the abundance of environmental objects that naturally interact with wind, such as trees, flags, and clothing. This initial pilot study aims to address this challenge by examining tree movement using two consecutive techniques: (1) optical flow to extract the natural movement vectors, and (2) deep recurrent neural networks to translate the vectors into wind velocity. The proposed CNN-ConvLSTM model, trained on a video dataset encompassing diverse environmental conditions with ground wind speeds from 0 to 14.6 m/s, extracted visual and motion features from RGB and optical flow images, achieving an 87.42% prediction accuracy in capturing spatiotemporal wind-induced motion patterns. These results suggest the possibility of extending visual anemometer technology to broader scenarios and diverse natural objects, guaranteeing safer UAV operation in complex environments.

## I. INTRODUCTION

Urban Air Mobility (UAM) is a rapidly advancing field that has garnered significant attention from industry and academia. A wide variety of Unmanned Aerial Vehicles (UAVs) have been developed for applications such as recreational use, delivery, photography, and sports [1]. Despite their versatility, UAVs face limitations such as reduced flight speeds, lightweight frames, small form factors, and low-altitude operations. These factors make them notably vulnerable to wind disturbances [2]. These challenges are particularly pronounced in urban environments, where complex and dynamic near-surface geography [3], including obstacles such as buildings and narrow corridors [4], creates unpredictable wind patterns and turbulence, further complicating UAV operations. The landing phase of UAV operations is particularly vulnerable to collisions, especially due to the complex and unpredictable conditions in urban environments [5], largely due to the unpredictable wind conditions prevalent in urban environments. Accurately estimating prevailing wind conditions in such complex settings during the critical landing phase of small to medium-sized UAVs remains a significant challenge.

### A. A State of the Art and Gaps

Recent research has increasingly focused on the modelling and measurement of near-surface wind fields, particularly in urban environments. CFD simulations and wind tunnel experiments with scaled city models have been widely applied in previous studies to analyze urban airflow dynamics [6], [7]. However, such approaches often oversimplify the complexities of urban wind dynamics, including turbulence and multi-scale interactions influenced by the heterogeneous urban landscape. To enhance the precision of wind speed estimation, data fusion techniques have been introduced [8], integrating measurements from multiple sources such as LiDAR and remote sensing technologies [9], [10]. While these methods offer high spatial accuracy over large areas, their applicability is constrained by substantial weight, power consumption, and operational costs. Alternatively, compact recording sensors can be mounted directly on UAVs [11], but their measurements are often compromised by rotor-induced airflow interference. And the limited payload capacity of small UAVs restricts their ability to carry more advanced or heavier instrumentation.

Several methods for visual wind estimation have been proposed, with the Beaufort wind scale being a known example [12]. This empirical approach classifies wind levels based on observable effects on natural objects, such as smoke, leaves, branches, and flags, enabling wind speed estimation without direct physical access to the target area. Trees, in particular, have been shown to reliably indicate wind speed and direction [13], as their motion dynamics exhibit consistent patterns across specific wind scales, with the magnitude of their movement correlating strongly with wind speed [14]. However, the Beaufort scale's reliance on discrete wind classes limits precision [15], and its dependence on subjective human observations introduces potential inaccuracies. To overcome these limitations, recent studies have adopted data-driven methods that utilize deep learning algorithms to analyze the motion of natural objects influenced by wind. By capturing and processing ground-based imagery or video, these approaches enable wind speed estimation and classification with automation [16]–[18]. Despite their promise, further work is needed to increase their accuracy and generalizability in a variety of environmental conditions. Building on this foundation, this study adopts a similar methodology with the objective of advancing visual anemometer techniques. This research aims to develop a robust and reliable solution for providing real-

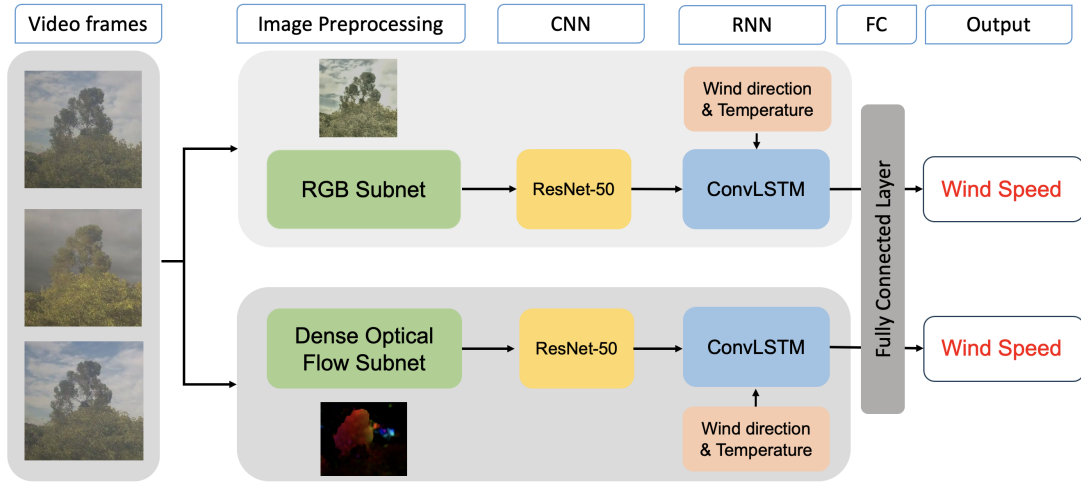


**Fig. 1:** Overview of the CNN-LSTM framework for wind velocity estimation. The model extracts spatial features from RGB and optical flow images using a CNN and models temporal dependencies using an LSTM.

time safety wind information during UAV landing operations, particularly in complex, resource-constrained, and dynamic urban settings.

### B. Innovation

Previous studies often used limited datasets, either confined to a single environment or lacking meteorological context, and mainly classified wind speed into discrete levels rather than predicting precise velocities.

To address these limitations, this study uses two distinct datasets to enhance model robustness and generalizability. The first dataset consists of fixed-scene, time-lapse videos spanning an extended period, providing a stable reference for long-term tree motion analysis. The second dataset comprises multi-scene, continuous video recordings, enabling the model to learn from dynamic environmental variations. Unlike prior work, our datasets incorporate additional meteorological parameters, such as temperature and wind direction, enriching the model’s input space and improving its predictive accuracy. In the initial phase, the fixed-scene dataset was used to establish a baseline model through optical flow-based motion analysis and deep learning optimization. The multi-scene dataset was subsequently employed to refine the model, ensuring it generalizes well across varying conditions and supports continuous wind speed prediction beyond discrete classifications. This dual-dataset strategy significantly improves the model’s capability to infer precise wind velocities across diverse environmental settings.

## II. METHODOLOGY

### A. Overview of the Approach

Accurate wind speed estimation is essential for safe UAV operations, particularly during takeoff and landing. This study leverages a CNN-ConvLSTM framework to extract spatiotemporal patterns from video data and infer wind velocity from the motion of natural objects. Fig. 1 illustrates the model

architecture, which consists of two main stages: (1) feature extraction from RGB and optical flow images using a CNN, and (2) temporal sequence modeling using an LSTM network.

### B. Dataset

To evaluate model performance, we constructed two datasets: NW3 (fixed observations: Fig. 2a) and CUW (mobile observations: Fig. 2b). The NW3 dataset consists of time-lapse videos captured from a fixed camera over an extended period, while the CUW dataset comprises multi-scene, continuous video recordings. Each dataset includes synchronized meteorological parameters (Fig. 3) such as wind speed, direction, and temperature, collected from networked weather stations, APIs, and handheld anemometers.

1) *NW3 Dataset:* The NW3 dataset was gathered at the NW3 Weather station in Hampstead, North London, UK [19]. A Hikvision DS-2CD2055FWD-I IP camera (4 mm focal length) recorded 1-minute-interval time-lapse videos, while a Davis Vantage Pro 2 station provided concurrent meteorological measurements. We focused on tree canopies (ash, sycamore, hepatica), yielding 1,440 frames per day. Each frame was cropped, resized ( $224 \times 224$ ), and normalized. To form input samples, we used 5 consecutive frames (sampled every 5 minutes), with wind speed as the primary label and gust speed, wind direction, and temperature as auxiliary features. Over a 31-day collection (October 2023–February 2024), wind speeds ranged from 0 m/s to 14.6 m/s, resulting in 44,640 labeled clips.

2) *CUW Dataset:* The CUW dataset was collected near four weather stations at Cranfield University (Bedford, UK). A Panasonic DC-S5M2 camera recorded daytime-only video over ten days in mid-November 2024 (frame rate: 25 fps, segmented into 3-second clips). Wind speeds ranged from 0 m/s to 12.6 m/s, with weather data refreshed every ten minutes using a WS-GP2 station and a GT8907 handheld anemometer. Target species included elm, red raspberry, birch, passionflower, sycamore, and balsam. Ultimately, 610 labelled

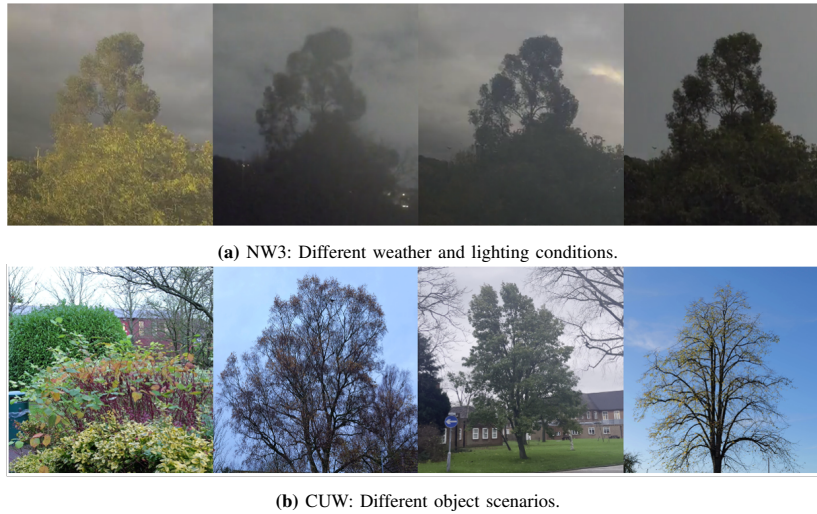


**Fig. 2:** Examples of cropped video frames from the dataset. (a) NW3 dataset under varying weather and lighting conditions; (b) CUW dataset featuring different target objects.

clips were obtained, each featuring synchronized wind speed, direction, and temperature annotations.

### C. Feature Extraction

Both pre-processed RGB maps and optical flow maps undergo feature extraction to capture spatial characteristics relevant to wind-induced motion. Natural objects in video frames exhibit spatiotemporal patterns that correlate with wind speed and direction. Spatial features, such as object characteristics and scene attributes [20], [21], are extracted from RGB images using a ResNet-based CNN. Additionally, motion features, including magnitude and direction, are computed from optical flow fields to capture the displacement and deformation of wind-affected objects [22].

This study employs ResNet-18 and ResNet-50 architectures as feature extractors. ResNet networks leverage residual blocks, which mitigate the vanishing gradient problem through skip connections. ResNet-50, with its deeper architecture and increased number of parameters, captures finer details compared to ResNet-18 [25]. However, its deeper structure also incurs higher computational and memory costs. In this study, ResNet is exclusively used for feature extraction without performing classification tasks. The extracted feature dimensions are  $5 \times 512$  for ResNet-18 and  $5 \times 2048$  for ResNet-50, both of which serve as inputs to the subsequent LSTM and ConvLSTM.

### D. Optical flow computing

Optical flow is employed to estimate motion vectors for each pixel by analyzing temporal changes in image intensity. Traditional optical flow algorithms primarily rely on brightness constancy assumptions between two consecutive frames [22], [26]. These algorithms are generally categorized into sparse and dense optical flow methods. Sparse optical flow focuses on key points, offering faster computation but lacking comprehensive global information. In contrast, dense optical flow

computes motion vectors for every pixel, providing a detailed motion field and excelling in motion estimation tasks [27].

As Fig. 4 shows, dense optical flow effectively captures the contours and motion dynamics of natural objects, such as trees. This detailed motion information can significantly contribute to wind speed estimation by enhancing the model’s ability to interpret wind-induced motion patterns.

### E. Network structure and implementation details

Wind speed prediction is formulated as a regression problem, to generate continuous wind speed values. The proposed CNN-LSTM model integrates: The CNN-ConvLSTM model includes a CNN (ResNet-18 or ResNet-50) to extract spatial features [23], [31], and an LSTM to capture temporal dependencies [24]. The fusion layer combines spatial and motion features for wind speed inference.

The training process utilizes the Mean Squared Error (MSE) as the loss function, offering a smooth and differentiable objective that strongly penalizes large deviations between predictions and targets [28].

To assess model performance, several evaluation metrics are adopted. The Mean Absolute Error (MAE) calculates the average magnitude of prediction errors. The Root Mean Squared Error (RMSE) emphasizes larger deviations by squaring the differences, providing sensitivity to outliers. The coefficient of determination ( $R^2$ ) quantifies the proportion of variance in wind speed explained by the model, with values approaching 1 indicating high explanatory power. Together, these metrics present a well-rounded evaluation of both predictive accuracy and generalization capacity.

The model was trained on a Google Colab PRO+ instance equipped with an NVIDIA A100 GPU (40GB VRAM) and 85GB RAM. Each training epoch required approximately 7 minutes and 39 seconds.

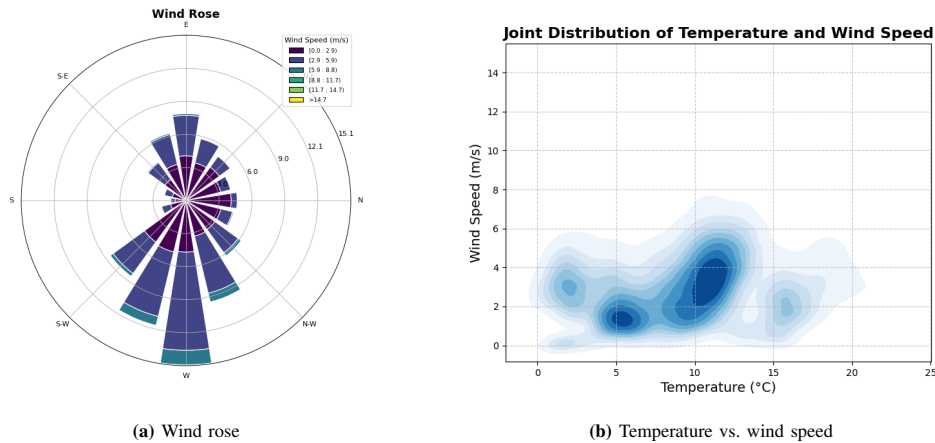


**Fig. 3:** Key weather data statistics. (a) Wind rose: Predominant wind directions are from the south and north, with fewer samples above 8 m/s. (b) Joint distribution of temperature and wind speed: Most temperatures range from 4–12 °C, and wind speeds from 1–4.5 m/s.

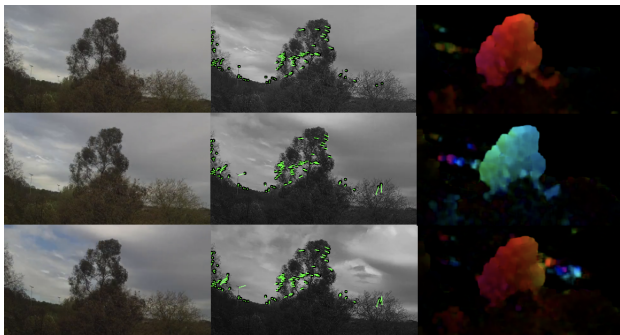


**Fig. 4:** Example of optical flow calculation for NW3 dataset. (a) Original RGB image; (b) Lucas-Kanade sparse optical flow computation; (c) Farneback dense optical flow calculation

The model was trained using the Adam optimizer with an initial learning rate of 0.001, adjusted dynamically via a ReduceLROnPlateau scheduler. To improve generalization, ConvLSTM layers used recurrent dropout (rate = 0.3), and batch normalization followed feature extraction. Early stopping (patience = 10 epochs) was applied to halt training when validation loss plateaued.

Hyperparameter tuning was conducted via Random Search, optimizing learning rate, LSTM units (128, 256, 512), and dropout rates. The NW3 dataset included two auxiliary features, while the CUW dataset incorporated seven (mean and difference of weather values), enriching contextual information and enhancing prediction robustness.

### III. RESULTS AND DISCUSSION

#### A. Comparison of CNN Backbones

We evaluated ResNet-18 and ResNet-50 for wind-speed prediction using RGB inputs and an LSTM with 256 hidden units. As shown in Table I, ResNet-50 yielded lower MAE and RMSE, along with higher  $R^2$  and accuracy, compared to ResNet-18. Although ResNet-18 requires fewer computational resources, its higher error and lower accuracy make it less ideal for precise wind estimation. Thus, ResNet-50 was

chosen for subsequent experiments due to its stronger overall performance

**TABLE I:** Performance Comparison of CNN Architectures, “Acc.” denotes the percentage of predictions within  $\pm 1.0$  m/s of the ground truth (i.e., accuracy).

Model	MAE (m/s)	RMSE (m/s)	$R^2$	Acc. (%)
ResNet-18	0.871	0.935	0.591	65.8
ResNet-50	<b>0.560</b>	<b>0.742</b>	<b>0.799</b>	<b>83.8</b>

#### B. Evaluation of Recurrent Models and Architectural Variations

We next examined how different recurrent architectures affect wind-speed estimation, experimenting with LSTM, GRU, ConvLSTM, and Transformer-based networks. Our evaluation considered accuracy, inference time, and robustness to varying data sampling strategies and feature sets.

1) *Dataset Partitioning and Data Distribution:* We stratified the dataset by wind-speed range, temperature, and wind direction to ensure balanced coverage of seasonal and weather variations. This approach minimizes bias toward specific wind conditions and enhances model generalization.

2) *Impact of Hidden Units and Computational Trade-offs:* The ResNet-50 + LSTM model was evaluated with different numbers of hidden units. As shown in Table II, the model with 256 hidden units provides the best trade-off between computational efficiency and accuracy. These results highlight the importance of selecting an appropriate model complexity to avoid overfitting while ensuring generalization.

**TABLE II:** Effect of Hidden Units on Accuracy and Inference Time

Hidden Units	Acc. (%)	Time (s/batch)
128	75.2	0.36
256	<b>83.8</b>	1.52
512	76.3	5.68
1024	73.2	24.7

3) *Comparison with State-of-the-Art Recurrent Models:* We then compared LSTM-based methods with GRU, ConvLSTM, and a Transformer-based network (Table III). ConvLSTM achieves the best overall metrics, while LSTM serves as a solid baseline and GRU performs slightly worse. In contrast, the Transformer model exhibits lower accuracy and longer training times (8.19 s/iteration), making it less practical for this dataset.

TABLE III: Comparison of Recurrent Architectures

Model	MAE (m/s)	RMSE (m/s)	$R^2$	Acc. (%)
LSTM	0.560	0.742	0.799	83.8
GRU	0.643	0.828	0.812	81.1
ConvLSTM	0.550	0.717	0.846	<b>84.5</b>
Transformer	0.778	0.871	0.750	69.3

The results indicate that ConvLSTM achieves the best overall performance, while LSTM serves as a strong baseline, and GRU performs slightly worse across all metrics. The Transformer-based approach underperforms in both accuracy and error metrics, with significantly longer training time, making it less suitable for this dataset.

### C. Addition of auxiliary features and Optical flow calculation

1) *Feature Selection and Robustness Analysis:* To assess the robustness of our approach, we further conducted experiments by adding or removing features, altering image sizes, and modifying sampling strategies. The removal of wind direction features led to an 8.4% drop in accuracy while reducing image resolution by 50% resulted in a 6.9% performance degradation. These findings highlight the importance of comprehensive feature representation for robust wind speed prediction.

TABLE IV: Impact of Optical Flow on Accuracy by Dataset

Dataset	Acc. RGB (%)	Acc. Opt. Flow (%)
NW3	84.5	<b>87.4</b>
CUW	81.6	83.7

Following the exploration, we identified suitable parameters and training strategies for the proposed model. ResNet-50 was selected as the CNN backbone to reduce training time and mitigate overfitting. And ConvLSTM was chosen, striking a balance between computational efficiency and accuracy.

As shown in Table IV, the addition of optical flow significantly improved model accuracy. The NW3 dataset accuracy increased by 2.95%, while the CUW dataset improved by 2.14%. This enhancement can be attributed to the dynamic motion cues provided by optical flow, which allow the model to better capture wind speed changes and directional variations.

Overall, integrating auxiliary features contributed to additional performance gains, demonstrating that leveraging multi-source data enhances model generalization. These findings emphasize the critical role of optical flow in wind speed

estimation, making it a valuable feature for future deep-learning-based meteorological applications.

### D. Results of the model

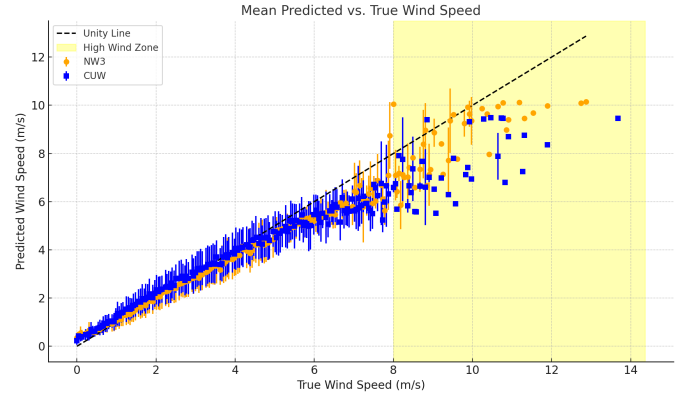


Fig. 5: Average predictions of the model tester. Each data point represents the average forecast performance across a specific wind speed interval, with error bars indicating the standard deviation of the predicted wind speeds. The dashed line corresponds to the ideal predicted wind speed values. The yellow-shaded region represents high wind speed intervals (greater than 8 m/s), which are also areas of limited sample availability.

TABLE V: Accuracy (%) by Wind Speed Category: Low (0–5 m/s), Medium (5–10 m/s), and High (>10 m/s).

Dataset	Low Wind	Medium Wind	High Wind
NW3	96.5	89.3	74.8
CUW	94.7	85.2	66.9

Fig. 5 plots the model’s average predictions across wind-speed intervals. While both datasets show high accuracy at lower speeds, performance degrades beyond 10 m/s, reflecting the limited number of high-wind samples (Table V). Consequently, variance increases in that range due to data imbalance.

Based on the comparison with the results reported by Cardona et al. [17], our models demonstrate superior accuracy across NW3 datasets (Table VI). These results highlight the robustness of our models in capturing wind speed variations while maintaining high accuracy. The improvement is likely due to the integration of optical flow features and more advanced temporal modelling techniques, which enhance the ability to generalize across varying wind conditions.

## IV. CONCLUSION

This study demonstrates the potential of computer vision and deep learning techniques for inferring near-ground wind velocity to enhance UAV safety, particularly during the landing phase in complex urban environments. Two datasets with synchronized video and weather data were developed, and a CNN-ConvLSTM-based framework was proposed to infer wind speed from the motion of natural objects. The models achieved satisfactory prediction performance across a 0–14.6 m/s wind speed range, indicating strong applicability for real-world scenarios.

TABLE VI: Performance Comparison with Prior Work

Model	RMSE (m/s)	Acc. (%)
Cardona et al.	1.47	85.7
Ours (NW3)	0.701	<b>87.4</b>
Ours (CUW)	0.836	83.7

However, model accuracy degrades under high wind conditions (above 10 m/s), primarily due to data imbalance. Future research should explore strategies such as data augmentation and synthetic video generation to enrich the data set [29], [30], especially under extreme conditions. Additionally, incorporating alternative wind-responsive objects, such as flags, smoke, or flexible structures, may improve model generalizability across varied urban contexts. Further validation under real UAV flight conditions and turbulent weather scenarios will be essential to assess robustness and operational reliability. These improvements would help establish the method as a practical and scalable solution for onboard or ground-based UAV wind sensing.

#### REFERENCES

- [1] C. Lee, S. Kim, and B. Chu, "A survey: Flight mechanism and mechanical structure of the UAV," *International Journal of Precision Engineering and Manufacturing*, vol. 22, no. 4, pp. 719–743, 2021.
- [2] B. H. Wang, D. B. Wang, Z. A. Ali, B. Ting Ting, and H. Wang, "An overview of various kinds of wind effects on unmanned aerial vehicle," *Measurement and Control*, vol. 52, no. 7-8, pp. 731–739, 2019.
- [3] E. Ranquist, M. Steiner, and B. Argrow, "Exploring the range of weather impacts on UAS operations," in *18th Conference on Aviation, Range and Aerospace Meteorology*, Seattle, WA, 2017.
- [4] Y. Qian, T. C. Chakraborty, J. Li, D. Li, C. He, C. Sarangi, et al., "Urbanization impact on regional climate and extreme weather: Current understanding, uncertainties, and future research directions," *Advances in Atmospheric Sciences*, vol. 39, no. 6, pp. 819–860, 2022.
- [5] G. Wild, J. Murray, and G. Baxter, "Exploring civil drone accidents and incidents to help prevent potential air disasters," *Aerospace*, vol. 3, no. 3, p. 22, 2016.
- [6] G. Kang, J.-J. Kim, and W. Choi, "Computational fluid dynamics simulation of tree effects on pedestrian wind comfort in an urban area," *Sustainable Cities and Society*, vol. 56, p. 102086, 2020.
- [7] M. Yin and B. J. He, "Performance-based urban ventilation corridor for actual achievement of environmental benefits," *Building and Environment*, vol. 240, p. 112536, 2025.
- [8] W. Guo, H. Du, C. Guo, B. J. Southwell, J. W. Cheong, and A. G. Dempster, "Information fusion for GNSS-r wind speed retrieval using statistically modified convolutional neural network," *Remote Sensing of Environment*, vol. 272, p. 112934, 2022.
- [9] F. Shen, Z. Shu, J. Dong, G. Jin, L. Yang, Z. Hui, and H. Xu, "Parameter study on ultraviolet Rayleigh–Brillouin Doppler lidar with dual-pass dual Fabry–Perot interferometer for accurately measuring near-surface to lower stratospheric wind field," *Photonics*, vol. 12, no. 1, p. 92, Jan. 2025.
- [10] A. Naqvi, A. Ali, W. A. Altabay, and S. A. Kouritem, "Energy harvesting from fluid flow using piezoelectric materials: A review," *Energies*, vol. 15, no. 19, p. 7424, 2022.
- [11] D. Yeo, N. Sydney, and D. A. Paley, "Onboard flow sensing for rotary-wing UAV pitch control in wind," in *AIAA guidance, navigation, and control conference*, 2016, p. 1386.
- [12] S. Pomahiya, N. Nurwan, N. I. Yahya, S. K. Nasib, I. K. Hasan, and A. Asriadi, "Wind speed category characteristics in Bone Bolango Regency: A Markov chain approach using the Beaufort scale and Metropolis-Hastings algorithm," *Pattimura International Journal of Mathematics (PIJMATH)*, vol. 3, no. 2, pp. 63–68, 2024.
- [13] S. J. Mitchell, "Wind as a natural disturbance agent in forests: A synthesis," *Forestry*, vol. 86, no. 2, pp. 147–157, 2013.
- [14] A. Mascitelli, V. Coletta, P. Bombi, B. De Cinti, S. Federico, G. Matteucci, A. Mazzoni, V. G. Mazzini, I. Petenko, and S. Dietrich, "Tree motion: Following the wind-induced swaying of arboreal individuals using a gnss receiver," *Italian Journal of Agrometeorology*, vol. 5, no. 3, pp. 25–36, 2019.
- [15] S. Fan, M. D. Wykes, W. E. Lin, R. L. Jones, A. G. Robins, and P. F. Linden, "A full-scale field study for evaluation of simple analytical models of cross ventilation and single-sided ventilation," *Building and Environment*, vol. 187, p. 107386, 2021.
- [16] J. O. Dabiri, M. F. Howland, M. K. Fu, and R. H. Goldshmid, "Visual anemometry for physics-informed inference of wind," *Nature Reviews Physics*, vol. 5, no. 10, pp. 597–611, 2023.
- [17] J. Cardona, M. F. Howland, and J. Dabiri, "Seeing the wind: Visual wind speed prediction with a coupled convolutional and recurrent neural network," *Advances in Neural Information Processing Systems*, vol. 32, 2019.
- [18] Q. Zhang, J. Xu, M. Crane, and C. Luo, "See the wind: Wind scale estimation with optical flow and visualwind dataset," *Science of The Total Environment*, vol. 846, p. 157204, 2022.
- [19] B. Masschelein-Rodgers, "Nw3 weather," <http://nw3weather.co.uk>
- [20] A. Hichri, M. Mansouri, M. Hajji, K. Bouzrara, H. Nounou, and M. Nounou, "Fault classification using deep learning in a grid-connected photovoltaic system," in *Proc. 2022 8th Int. Conf. Control, Decis. Inf. Technol. (CoDIT)*, vol. 1, May 2022, pp. 1312–1317.
- [21] K. Simonyan and A. Zisserman, "Very deep convolutional networks for large-scale image recognition," *arXiv preprint arXiv:1409.1556*, 2014.
- [22] M. Zhai, X. Xiang, N. Lv, and X. Kong, "Optical flow and scene flow estimation: A survey," *Pattern Recognition*, vol. 114, p. 107861, 2021.
- [23] K. Simonyan and A. Zisserman, "Two-stream convolutional networks for action recognition in videos," in *Advances in Neural Information Processing Systems*, vol. 27, 2014, pp. 568–576.
- [24] J. Yue-Hei Ng, M. Hausknecht, S. Vijayanarasimhan, O. Vinyals, R. Monga, and G. Toderici, "Beyond short snippets: Deep networks for video classification," in *Proceedings of the IEEE Conference on Computer Vision and Pattern Recognition (CVPR)*, 2015, pp. 4694–4702.
- [25] D. Hindarto, "Comparison of detection with transfer learning architecture resnet18, resnet50, resnet101 on corn leaf disease," *Jurnal Teknologi Informasi Universitas Lambung Mangkurat (JTIULM)*, vol. 8, no. 2, pp. 41–48, 2023.7
- [26] J. Wulff and M. J. Black, "Efficient sparse-to-dense optical flow estimation using a learned basis and layers," in *Proceedings of the IEEE Conference on Computer Vision and Pattern Recognition*, 2015, pp. 120–130.
- [27] T. Brox and J. Malik, "Large displacement optical flow: descriptor matching in variational motion estimation," *IEEE Transactions on pattern analysis and Machine Intelligence*, vol. 33, no. 3, pp. 500–513, 2010.
- [28] M. Mathieu, C. Couprie, and Y. LeCun, "Deep multi-scale video prediction beyond mean square error," *arXiv preprint arXiv:1511.05440*, 2015.
- [29] E. K. Al-Bwana, I. Sayahi, M. Alauthman, and M. A. Mahjoub, "Adversarial network augmentation and tabular data for a new COVID-19 diagnostics approach," in *Proc. 2024 10th Int. Conf. Control, Decis. Inf. Technol. (CoDIT)*, Jul. 2024, pp. 2000–2005.
- [30] C. Bowles, L. Chen, R. Guerrero, P. Bentley, R. Gunn, A. Hammers, D. A. Dickie, M. V. Hernández, J. Wardlaw, and D. Rueckert, "Gan augmentation: Augmenting training data using generative adversarial networks," *arXiv preprint arXiv:1810.10863*, 2018.
- [31] N. M. Bhiri, S. Ameur, I. Jegham, I. Alouani, and A. B. Khalifa, "A deep CNN-BiGRU network for multi-stream hand gesture recognition framework," in *Proc. 2024 10th Int. Conf. Control, Decis. Inf. Technol. (CoDIT)*, Jul. 2024, pp. 893–898.